V European Conference on Computational Fluid Dynamics
ECCOMAS CFD 2010
J. C. F. Pereira and A. Sequeira (Eds)
Lisbon, Portugal,14-17 June 2010

REYNOLDS STRESS MODELLING FOR COMPLEX AERODYNAMIC FLOWS

Bernhard Eisfeld*

*German Aerospace Center (DLR)
Institute of Aerodynamics and Flow Technology
Lilienthalplatz 7, D-38108 Braunschweig, Germany
e-mail: bernhard.eisfeld@dlr.de

Key words: Turbulence modelling, Differential Reynolds Stress Model, Aerodynamics

Abstract. *A differential Reynolds stress model is presented that combines the Speziale-Sarkar-Gatski (SSG) model with the Launder-Reece-Rodi (LRR) model near walls, where the length scale is provided by Menter's baseline ω-equation. The model is applied to transonic flows around the RAE 2822 airfoil, the ONERA M6 wing and the DLR-ALVAST generic aircraft. Improved prediction of shock and pressure induced separation is observed compared to standard eddy viscosity models.*

1 INTRODUCTION

Industrial engineering is increasingly relying on computational simulation data. In particular, in aerodynamic aircraft design there is a trend towards simulation based design where Computational Fluid Dynamics (CFD) is employed for reducing wind tunnel tests to only a few targeted key experiments. Obviously this strategy relies on the predictive accuracy of the respective simulation tools and thus the available physical models in a wide range of flight conditions. Hence turbulence modelling is a key technology for providing sufficiently accurate predictions, particularly at the boundaries of the flight envelope.

Besides accuracy efficiency is a key criterion in industrial engineering, because of the large amount of simulation data needed in design and optimisation. Direct Numerical Simulations (DNS) and Large Eddy Simulations (LES), accurately resolving all or part of the turbulent fluctuations in space and time, are therefore currently beyond the scope for data production in routine applications. Instead, methods based on the Reynolds averaged Navier-Stokes (RANS) equations supplemented with corresponding turbulence models are still the backbone of industrial CFD applications.

In the RANS approach only the average effect of turbulence on the mean flow is considered, where the so-called Reynolds stress tensor, representing the average fluctuations of the velocity field, has to be modelled in terms of mean flow quantities. The typical modelling approach relies on the Boussinesq hypothesis, assuming turbulence to effectively increase the viscosity of a Newtonian fluid, where the additional so-called eddy viscosity is not a property of the fluid, but depends on the flow.

In the past algebraic eddy viscosity models like the Baldwin-Lomax model [1] have been popular in aeronautical applications, where the eddy viscosity is computed directly from the mean flow field, whereas today transport equation models are state-of-the-art, where the eddy viscosity is computed from the transported quantities. Because of there advantages near the wall k-ω type models like the one by Wilcox [13] or particularly the Shear Stress Transport (SST) model by Menter [7, 8] are preferred in aeronautics to the otherwise popular k-ϵ type models. Alternatively the Spalart-Allmaras model [10, 11] is widely applied, involving only one transport equation for a modified eddy viscosity.

These eddy viscosity models are well established in numerical aerodynamics and yield reliable predictions as long as the flow stays attached. However discrepancies with experiments are observed in case of separation, as is typical of approaching the boundaries of the flight envelope. Key scenarios are the shock-boundary layer interaction at high speed flight and low speed conditions close to maximum lift.

The failure of eddy viscosity models in case of separation can be associated with the Boussinesq hypothesis, enforcing the predicted Reynolds stresses being parallel to the viscous stresses. Furthermore this approach leads to isotropic normal stresses near walls which is in contrast to experimental observation.

A possible remedy consists in replacing the Boussinesq hypothesis by directly solving the transport equations for the individual Reynolds stresses. These equations can be

derived from the momentum equations and involve several terms associated with different phenomena that can be modelled according to physical reasoning. However, in contrast to standard eddy viscosity models, the production term of the Reynolds stress transport equation is exact and thus also includes effects of curvature and rotation. This feature makes the so-called Differential Reynolds Stress Models (DRSM) particularly promising for predicting complex flows in aerodynamics.

2 REYNOLDS STRESS MODELLING

The transport equation of the Reynolds stresses for compressible flow reads in general form

$$\frac{\partial}{\partial t}\left(\overline{\rho}\widetilde{R}_{ij}\right)+\frac{\partial}{\partial x_k}\left(\overline{\rho}\widetilde{U}_k\widetilde{R}_{ij}\right)=\overline{\rho}P_{ij}+\overline{\rho}\Phi_{ij}-\overline{\rho}\epsilon_{ij}+\overline{\rho}D_{ij}+\overline{\rho}M_{ij}, \tag{1}$$

where ρ is the density and U_i the components of the velocity vector. The overbar represents simple and the tilde mass weighted averages.

The components of the Reynolds stress tensor are defined as

$$\overline{\rho}\widetilde{R}_{ij}=\overline{\rho u_i'' u_j''}, \tag{2}$$

where the u_i'' denote the velocity fluctuations around the mass weighted mean. The trace of the specific Reynolds stress tensor is related to the specific kinetic turbulence energy $\widetilde{k}$ by

$$\widetilde{k}=\frac{\widetilde{R}_{ii}}{2}. \tag{3}$$

As already stated, the production term of the Reynolds stress transport equation (1)

$$\overline{\rho}P_{ij}=-\overline{\rho}\widetilde{R}_{ik}\frac{\partial\widetilde{U}_j}{\partial x_k}-\overline{\rho}\widetilde{R}_{jk}\frac{\partial\widetilde{U}_i}{\partial x_k} \tag{4}$$

is exact, since it does not involve any additional unknowns.

Various models exist for the re-distribution term $\overline{\rho}\Phi_{ij}$, where in the former aeronautics oriented EU-project FLOMANIA [5] the model by Speziale, Sarkar and Gatski (SSG) [12] has been considered the most promising one. However this model requires an ϵ-equation for providing the length scale. In contrast, Wilcox [14] has shown that the model by Launder, Reece and Rodi (LRR) [6] can be combined with an ω-equation for the length scale, when the so-called wall-reflexion terms are omitted. Both models can be cast into the same form reading

$$\begin{aligned}\overline{\rho}\Phi_{ij} &= -\left(C_1\overline{\rho}\epsilon+\frac{1}{2}C_1^*\overline{\rho}P_{kk}\right)\widetilde{b}_{ij}+C_2\overline{\rho}\epsilon\left(\widetilde{b}_{ik}\widetilde{b}_{kj}-\frac{1}{3}\widetilde{b}_{mn}\widetilde{b}_{mn}\delta_{ij}\right)\\ &\quad+\left(C_3-C_3^*\sqrt{II}\right)\overline{\rho}\widetilde{k}\widetilde{S}_{ij}^*+C_4\overline{\rho}\widetilde{k}\left(\widetilde{b}_{ik}\widetilde{S}_{jk}+\widetilde{b}_{jk}\widetilde{S}_{ik}-\frac{2}{3}\widetilde{b}_{mn}\widetilde{S}_{mn}\delta_{ij}\right)\\ &\quad+C_5\overline{\rho}\widetilde{k}\left(\widetilde{b}_{ik}\widetilde{W}_{jk}+\widetilde{b}_{jk}\widetilde{W}_{ik}\right),\end{aligned} \tag{5}$$

where

$$\widetilde{b}_{ij} = \frac{\widetilde{R}_{ij}}{2\widetilde{k}} - \frac{\delta_{ij}}{3} \tag{6}$$

are the components of the anisotropy tensor with its second invariant

$$II = \widetilde{b}_{ij}\widetilde{b}_{ij}, \tag{7}$$

and δ_{ij} denotes the components of the Kronecker tensor.

$$\widetilde{S}_{ij} = \frac{1}{2}\left(\frac{\partial \widetilde{U}_i}{\partial x_j} + \frac{\partial \widetilde{U}_j}{\partial x_i}\right) \qquad \text{and} \qquad \widetilde{S}^*_{ij} = \widetilde{S}_{ij} - \frac{\partial \widetilde{U}_k}{\partial x_k}\delta_{ij} \tag{8}$$

are the components of the mean strain rate tensor and its traceless counterpart, respectively, and

$$\widetilde{W}_{ij} = \frac{1}{2}\left(\frac{\partial \widetilde{U}_i}{\partial x_j} - \frac{\partial \widetilde{U}_j}{\partial x_i}\right) \tag{9}$$

represents the components of the mean rotation tensor. Finally the isotropic dissipation rate ϵ is linked to the specific dissipation rate ω by

$$\epsilon = C_\mu \widetilde{k}\omega, \tag{10}$$

where $C_\mu = 0.09$.

The dissipation term is usually modelled by an isotropic tensor according to

$$\overline{\rho}\epsilon = \frac{2}{3}\overline{\rho}\epsilon\delta_{ij} = \frac{2}{3}C_\mu \overline{\rho}\widetilde{k}\omega\delta_{ij} \tag{11}$$

and the diffusion term by a generalised gradient diffusion according to Daly and Harlow [3]

$$\overline{\rho}D_{ij} = \frac{\partial}{\partial x_k}\left[\left(\overline{\mu}\delta_{kl} + C_s\frac{\overline{\rho}\widetilde{k}}{\epsilon}\widetilde{R}_{kl}\right)\frac{\partial \widetilde{R}_{ij}}{\partial x_l}\right] = \frac{\partial}{\partial x_k}\left[\left(\overline{\mu}\delta_{kl} + \frac{C_s}{C_\mu}\frac{\overline{\rho}}{\omega}\widetilde{R}_{kl}\right)\frac{\partial \widetilde{R}_{ij}}{\partial x_l}\right], \tag{12}$$

where $\overline{\mu}$ is the average molecular viscosity of the fluid.

The contribution of the fluctuating mass flux, $\overline{\rho}M_{ij}$, due to density fluctuations are usually neglected, when considering transonic flows.

As on can see, all model terms can be alternatively expressed in terms of ϵ or ω. This allows transferring the ideas of Menter [7, 8] for combining a k-ω model near the wall with a k-ϵ model further away to differential Reynolds stress models.

In Menter's baseline model (BSL) the length scale is given by a single transport equation for ω

$$\frac{\partial\left(\overline{\rho}\omega\right)}{\partial t} + \frac{\partial}{\partial x_k}\left(\overline{\rho}\widetilde{U}_k\omega\right) = \alpha\frac{\omega}{\widetilde{k}}\frac{\overline{\rho}P_{kk}}{2} - \beta\overline{\rho}\omega^2 + \frac{\partial}{\partial x_k}\left[\left(\overline{\mu} + \sigma\frac{\overline{\rho}\widetilde{k}}{\omega}\right)\frac{\partial\omega}{\partial x_k}\right] + \sigma_d\frac{\overline{\rho}}{\omega}\max\left(\frac{\partial\widetilde{k}}{\partial x_k}\frac{\partial\omega}{\partial x_k}; 0\right), \tag{13}$$

where all coefficients continuously change according to

$$\phi = F_1 \phi^{(k-\omega)} + (1 - F_1)\, \phi^{(k-\epsilon)}, \tag{14}$$

using Menter's blending function

$$F_1 = \tanh\left(\zeta^4\right) \tag{15}$$

with

$$\zeta = \min\left[\max\left(\frac{\sqrt{\widetilde{k}}}{C_\mu \omega d}; \frac{500\overline{\mu}}{\overline{\rho}\omega d^2}\right); \frac{4\sigma^{(k-\epsilon)}\overline{\rho}\widetilde{k}}{\max\left\{2\sigma^{(k-\epsilon)}\frac{\overline{\rho}}{\omega}\frac{\partial\widetilde{k}}{\partial x_k}\frac{\partial\omega}{\partial x_k}; 10^{-20}\right\} d^2}\right] \tag{16}$$

and d the wall distance. The corresponding bounding values of the coefficients in the k-ϵ and the k-ω region are given in Tab. 1.

	α	β	σ	σ_d
k-ϵ	0.44	0.0828	0.856	$2\sigma^{(k-\epsilon)}$
k-ω	0.5556	0.075	0.5	0

Table 1: Values of coefficients of Menter's baseline ω-equation corresponding to the k-ϵ and k-ω parts.

The so-called SSG/LRR-ω model [4] adopts Menter's technique by changing the coefficients of the re-distribution and diffusion term accordingly from the LRR values at the wall to the SSG values further apart, i. e.

$$\phi = F_1 \phi^{(LRR)} + (1 - F_1)\, \phi^{(SSG)}, \tag{17}$$

The corresponding values of the coefficients in the LRR and SSG region are given Tab. 2.

	C_1	C_1^*	C_2	C_3	C_3^*	C_4	C_5	C_s
SSG	3.4	1.8	4.2	0.8	1.3	1.25	0.4	0.22
LRR	3.6	0	0	0.8	0	$\frac{18C_2^{(LRR)}+12}{11}$	$\frac{-14C_2^{(LRR)}+20}{11}$	$0.5C_\mu$

Table 2: Values of closure coefficients for the SSG and the LRR contributions to the SSG/LRR-ω re-distribution term. $C_2^{(LRR)} = 0.5556$, $C_\mu = 0.09$.

Combining this modelling for the Reynolds stresses with Menter's BSL ω-equation (13) yields a consistent change from the stress-ω model by Wilcox [14] near walls (= LRR without wall-reflexion) to the ϵ-based SSG model further away. As it appears, the SSG/LRR-ω is applicable to aerodynamic problems up to rather high complexity.

3 AERODYNAMIC APPLICATIONS

3.1 RAE 2822 Airfoil

The RAE 2822 airfoil is a standard test case for applying turbulence models at transonic speed [2]. In particular the conditions of the so-called Case 9 (Mach number $Ma = 0.73$, Reynolds number $Re = 6.5 \cdot 10^6$, incidence $\alpha = 2.8^0$) and Case 10 (Mach number $Ma = 0.75$, Reynolds number $Re = 6.2 \cdot 10^6$, incidence $\alpha = 2.8^0$) are regularly tested, where the challenge is to match the shock position in both cases sufficiently well.

Fig. 1 shows the pressure distributions obtained with three different turbulence models. As one can see, the Wilcox k-ω model yields the shock position downstream the experimental location and is far off for Case 10. In contrast the Menter SST as well as the SSG/LRR-ω model predict the shock for Case 9 slightly downstream and for Case 10 only slightly upstream the measured position, where it is difficult to judge which of both to prefer.

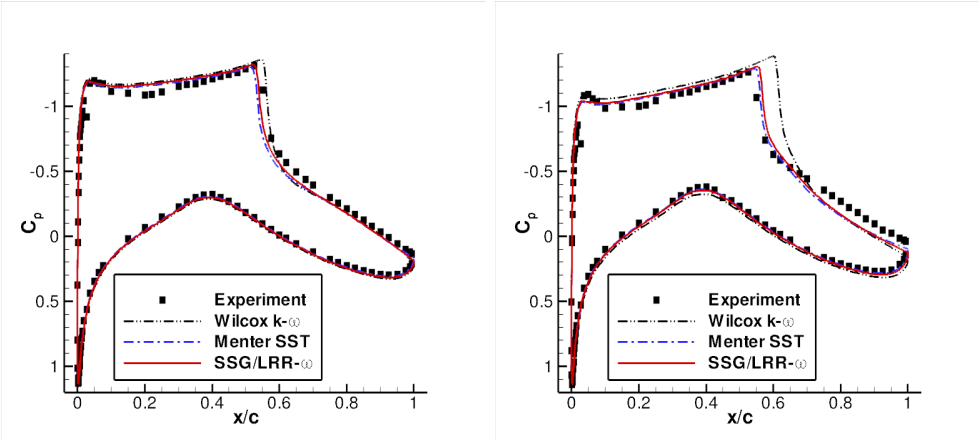

Figure 1: RAE 2822 airfoil. Pressure distributions for Case 9 (left) and Case 10 (right).

Nevertheless with two-equation models an unphysically high production of kinetic turbulence energy is observed near stagnation points. This so-called stagnation point anomaly is attributed to the fact that, in contrast to the Reynolds stress production term, the k-production term does not account for rotational effects. Fig. 2 shows the kinetic turbulence energy in the stagnation point region. Clearly the Menter SST model predicts a much higher level of k ahead the airfoil than the SSG/LRR-ω model, although production limiting is already applied, as suggested by Menter [7]. Fortunately in this particular case this effect has only little influence on the predicted shock position and is usually blanked out by setting transtion at the airfoil's nose.

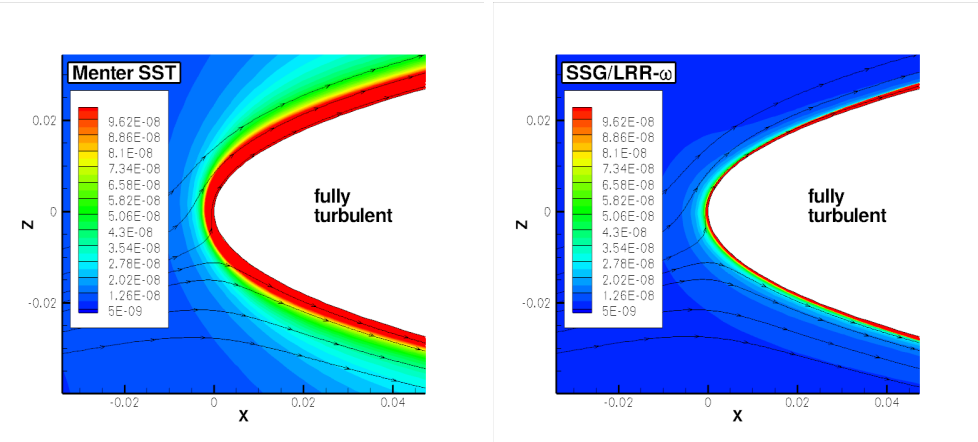

Figure 2: RAE 2822 airfoil, Case 9. Kinetic turbulence energy near stagnation point.

3.2 ONERA M6 Wing

The ONERA M6 wing is another standard test case for three-dimensional transonic flows [9]. The experiments have been carried out at a Mach number of $Ma = 0.84$ and a Reynolds number, based on the mean aerodynamic chord, of $Re = 11.72 \cdot 10^6$, where the angle of attack varied from $\alpha = 0.03^0$ to $\alpha = 6.06^0$. Most often results at $\alpha = 3.06^0$ are shown, where it comes out that the experimental pressure distribution is well predicted almost independently of the turbulence model [5].

However at the next higher experimental incidence of $\alpha = 4.08^0$ significant differences are observed between the results obtained with various turbulence models. Fig 3 shows the pressure distributions in two sections at 65% and 90% span, predicted by three different turbulence models in comparison with the experiments. Clearly the Reynolds stress model yields a good agreement with the measurements with some discrepancies at 65% span, where a double shock system is present. In contrast, all eddy viscosity models tested, except the Wilcox k-ω model (not shown here), show a large deviation from the measurement over most of the outer wing.

As can already been concluded from the pressure distributions, the failure of the Menter SST and Spalart-Allmaras model is due to a shock induced separation that is obviously over-estimated. Fig. 4 shows the friction lines, indicating the separation pattern, for the Spalart-Allmaras and the SSG/LRR-ω model. Clearly the latter predicts a much smaller separation region which is obviously in closer agreement with the experimental results.

3.3 DLR-ALVAST Generic Aircraft

The DLR-ALVAST model is a wing-body configuration that has been tested experimentally in the EU-project Enifair. Simulations have been carried out at a Mach number of $Ma = 0.75$ and a Reynolds number of $Re = 4.8 \cdot 10^6$, where the incidence has been adapted, until a lift coefficient of $C_L = 0.500$ has been achieved.

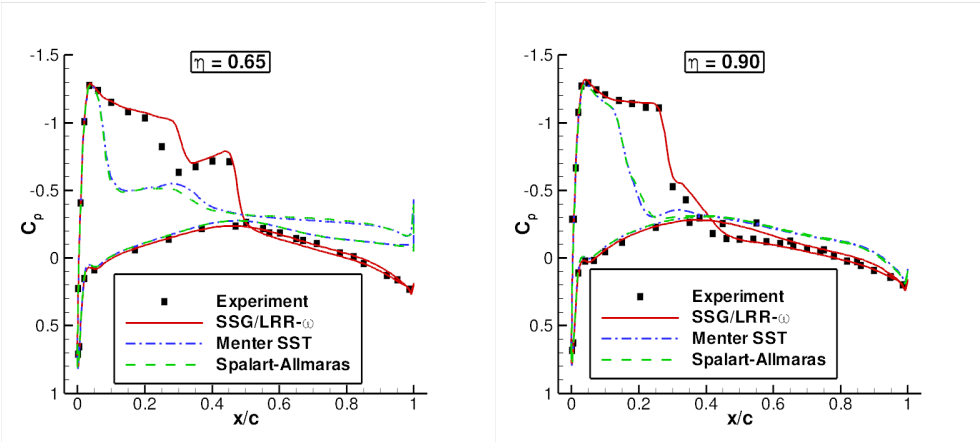

Figure 3: ONERA M6 wing. Pressure distributions at $\alpha = 4.08^0$.

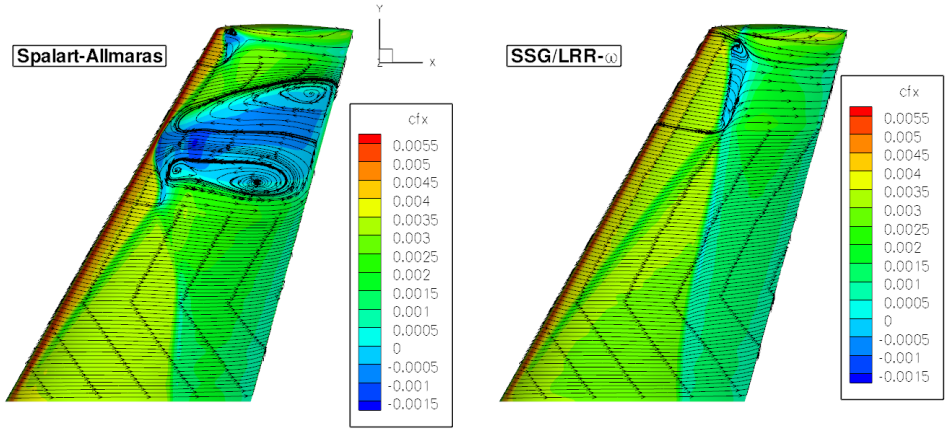

Figure 4: ONERA M6 wing, $\alpha = 4.08^0$. Friction lines on upper surface for Spalart-Allmaras model (left) and SSG/LRR-ω model (right).

Fig. 5 shows the friction lines on the upper surface of the ALVAST wing obtained with the Menter SST and the SSG/LRR-ω model. As one can see, the major difference occurs with respect to the separation in the wing-body junction which is predicted larger with the SST model. Comparing the inboard pressure distributions with the experiments, once again the Reynolds stress model yields somewhat better agreement than the eddy viscosity model, indicating higher accuracy with respect to the separation prediction.

4 CONCLUSIONS

A differential Reynolds stress modelling approach has been presented, combining the Speziale-Sarkar-Gatski (SSG) model [12] with the Launder-Reece-Rodi (LRR) model [6] near walls where the length scale is determined by Menter's baseline ω-equation [8]. This SSG/LRR-ω model is applicable to aerodynamic problems up to fairly high complexity.

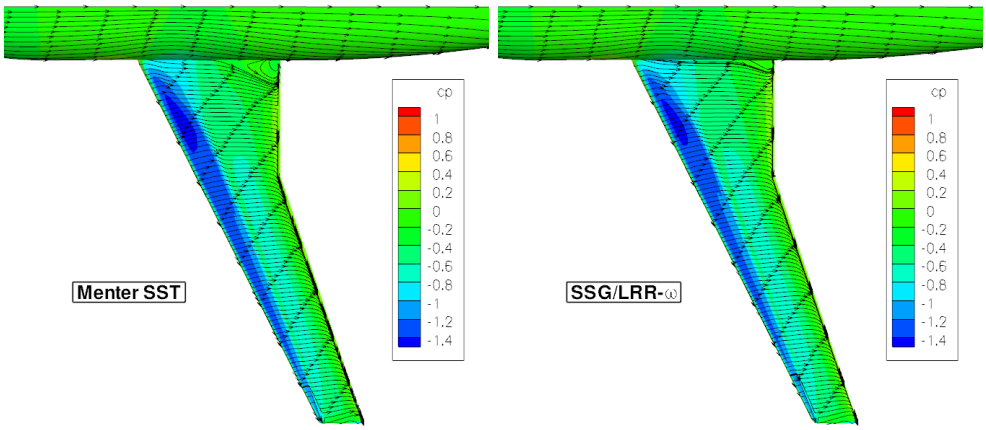

Figure 5: DLR-ALVAST generic aircraft, $C_L = 0.500$. Friction lines on upper surface for Menter SST (left) and SSG/LRR-ω model (right).

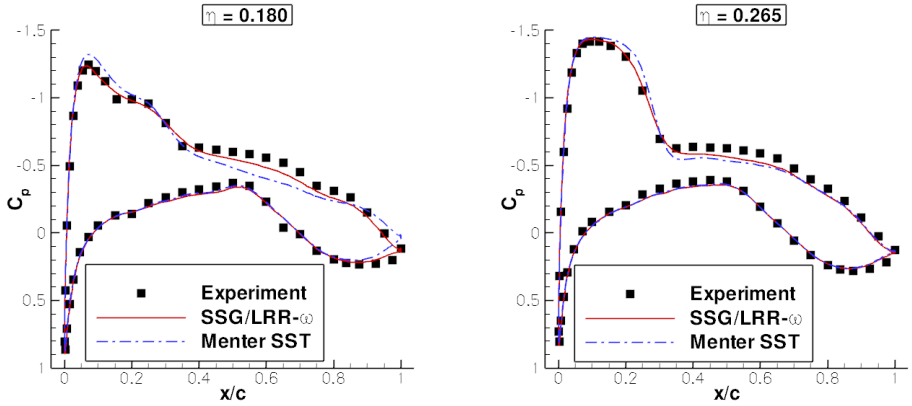

Figure 6: DLR-ALVAST generic aircraft, $C_L = 0.500$. Inboard pressure distributions at 18% and 26.5% span.

For the RAE 2822 airfoil the shock position of the so-called Case 9 and 10 is predicted similarly well as with the Menter SST eddy viscosity model. As to be expected due to the exact production term, the Reynolds stress model yields lower levels of kinetic turbulence energy ahead the stagnation point of the airfoil than the SST model, i. e. there is no stagnation point anomaly.

For the ONERA M6 wing at 4.08^0 angle of attack the SSG/LRR-ω model yields significantly better agreement with the experimental pressure distribution than the Menter SST and Spalart-Allmaras model. An over-prediction of shock induced separation by the eddy viscosity models has been identified as major source of the discrepancies. The Reynolds stress model predicts a much smaller separation region which is obviously in better agreement with the experiment.

Finally results have been presented for the DLR-ALVAST wing-body configuration at a given lift coefficient of $C_L = 0.500$. The predictions by the Menter SST and the

SSG/LRR-ω model differ mainly in the size of the separation in the wing-body junction which again is larger with the eddy viscosity model. Comparison of the inboard pressure distributions shows better agreement of the Reynolds stress model predicions with the experiment, indicating its higher accuracy in predicting complex separation.

REFERENCES

[1] B. S. Baldwin and H. Lomax, Thin Layer Approximation and Algebraic Model for Separated Turbulent Flows, *AIAA-Paper 78-0257* (1978).

[2] P. H. Cook, M. A. McDonald, and M. C. P. Firmin, Aerofoil RAE 2822 – Pressure Distributions, and Boundary Layer and Wake Measurements. In: J. Barche (Ed.), *Experimental Data Base for Computer Program Assessment*, AGARD Report AGARD-AR-138, Section A6 (1979).

[3] B. J. Daly and F. H. Harlow, Transport equations of turbulence, *Physics of Fluids* **13**, 2634–2649 (1970).

[4] B. Eisfeld and O. Brodersen, Advanced Turbulence Modelling and Stress Analysis for the DLR-F6 Configuration, *AIAA-Paper 2005-7727* (2005)

[5] W. Haase, B. Aupoix, U. Bunge and D. Schwamborn (Eds.), FLOMANIA – A European Initiative on Flow Physics Modelling, *Notes on Numerical Fluid Mechanics and Multidisciplinary Design*, **Vol. 94**, *Springer* (2006).

[6] B. E. Launder, G. J. Reece and W. Rodi, Progress in the development of a Reynolds-stress turbulence closure, *Journal of Fluid Mechanics* **68**, 537–566 (1975).

[7] F. R. Menter, Zonal Two Equation k-ω Turbulence Models for Aerodynamic Flows, *AIAA-Paper 93-2906* (1993).

[8] F. R. Menter, Two-Equation Eddy-Viscosity Turbulence Models for Engineering Applications, *AIAA Journal* **32**, 1598–1605 (1994).

[9] V. Schmitt and F. Charpin, Pressure Distributions on the ONERA-M6-Wing at Transonic Mach Numbers. In: J. Barche (Ed.), *Experimental Data Base for Computer Program Assessment*, AGARD Report AGARD-AR-138, Section B1 (1979).

[10] P. R. Spalart and S. R. Allmaras, A One-Equation Turbulence Model for Aerodynamic Flows, *AIAA-Paper 92-0439* (1992).

[11] P. R. Spalart and S. R. Allmaras, A One-Equation Turbulence Model for Aerodynamic Flows, *La Recherche Aérospatiale* **1**, 5–21 (1994).

[12] C. G. Speziale, S. Sarkar and T. B. Gatski, Modelling the pressure-strain correlation of turbulence: an invariant dynamical systems approach, *Journal of Fluid Mechanics*, **227**, 245–272 (1991).

[13] D. C. Wilcox, Reassessment of the Scale Determining Equation for Advanced Turbulence Models, *AIAA Journal* **26** 1299–1310 (1988).

[14] D. C. Wilcox, Turbulence Modeling for CFD, 2nd Edition, *DCW Industries* (1998).